Electron Autodetachment from Isolated Nickel and Copper Phthalocyanine−Tetrasulfonate Tetraanions: Isomer Specific Rates

Katharina Arnold,[†] Teodor Silviu Balaban,[†] Martine N. Blom,[†] Oli T. Ehrler,[‡] Stefan Gilb,[‡] Oliver Hampe,[†] Johan E. van Lier,[§] J. Mathias Weber,[‡] and Manfred M. Kappes*[,†,‡]

Institut für Nanotechnologie, Forschungszentrum Karlsruhe, P.O. Box 3640, D-76021 Karlsruhe, Germany, Institut für Physikalische Chemie, Universität Karlsruhe, Kaiserstr. 12, D-76128 Karlsruhe, Germany, and Faculty of Medicine, University of Sherbrooke, Sherbrooke, Québec, Canada

Received: September 25, 2002; In Final Form: December 2, 2002

Electron autodetachment from isolated metal phthalocyanine−tetrasulfonate tetraanions ($MPc(SO_3)_4^{4-}$) (M=Ni, Cu) was studied at room temperature in an FT-ICR mass spectrometer under UHV conditions. For M = Cu, the electron loss rate was measured for the as-prepared isomer mixture. In the case of M = Ni, two chromatographically purified fractions containing different compositions of constitutional isomers were studied. The observed rate constants for these fractions differed by a factor of 37 ± 5. Photoelectron spectroscopy indicates that both Cu and Ni compounds comprise isomer ensembles which are electronically metastable. Model calculations suggest that the differing electron loss rates observed for the Ni isomer fractions reflect tunneling through repulsive Coulomb barrier surfaces, which are themselves strongly isomer dependent in shape and height.

1. Introduction

Small multiply charged molecular anions (MCAs = multianions) are quite fragile and often metastable in the gas phase. The strong Coulombic repulsion between close-lying negative charges can result in spontaneous fragmentation, electron loss, or both. Nevertheless, as increasingly sophisticated experimental tools have become available, smaller and smaller multiply charged anions such C_n^{2-} ($n \geq 7$),[1] $S_2O_6^{2-}$,[2] $SO_4(H_2O)_n^{2-}$ ($n \geq 3$),[3] or MX_4^{2-} (M = Pt, Pd; X = Br, Cl)[4,5] have become accessible for gas phase studies. This has the added advantage of providing experimental benchmarks for small computationally tractable molecules against which evolving theoretical descriptions of multianion dynamics can be tested. In particular, the recent photoelectron spectroscopic measurements of Wang et al. have allowed fundamental insights into the characteristic electron detachment phenomena associated with multianions.[4,6]

$PtCl_4^{2-}$ is an example of a metastable dianion with a negative electron detachment energy (i.e., electronically unstable). In this case, spontaneous electron autodetachment may be observed on a time scale of seconds at room temperature.[5] This requires that the outgoing electron surmounts a nonlocal Coulomb barrier potential surface which is common, in a qualitative sense, to the ground and the excited states of all multianions. In principle, there are two mechanistic limits in which to think about this: (i) thermal electron emission (thermoemission) *over* the Coulomb barrier and (ii) tunneling *through* the Coulomb barrier, for the latter, a negative detachment energy is a necessary criterion.

In the case of thermal emission,[7] rate constants can be modeled using the unimolecular rate theory developed for thermoionization of neutral molecules (Klots theory) which is essentially dependent on the assumed magnitude of the Coulomb barrier, the size of the molecule, and the level of vibrational excitation. As first suggested by Landman et al.[8] for electronically unstable multianions, tunneling *through* a Coulomb barrier surface can be roughly described by the Wentzel−Kramers−Brillouin (WKB) approximation using the Coulomb barrier properties and the electron detachment energy. If both mechanisms are energetically possible, it is not clear a priori which one dominates. Consequently, in studying autodetachment, it is of interest to vary the excitation level. In our recent study of electron autodetachment from $PtCl_4^{2-}$, we have demonstrated that the level of vibrational excitation at room temperature is insufficient to allow for any thermoemission and that, therefore, the observed electron loss must be entirely attributable to electron tunneling.

Spontaneous electron loss from metastable multiply charged ions has also been theoretically investigated.[9,10] Both accurate initial and final state energies as well as aqequate descriptions of Coulomb barriers are crucial in order to quantitatively explain the experimentally observed electron autodetachment rates. Among other issues, the question of the localization/delocalization of the excess charges and the corresponding influence on the topology of the Coulomb barrier (e.g., 2D versus 3D) surface arises. Atomic clusters, which can be experimentally probed over a wide range of sizes and bonding types, are quite useful in this context. Examples of cluster MCAs with (partially) *delocalized* charge distributions, which have recently been studied experimentally, include (i) multiply charged metal cluster anions such as Ag_n^{2-} ($n > 28$)[11] or Pb_n^{3-} ($n > 76$)[12] and (ii) fullerene dianions C_n^{2-} ($n = 60$)[13,14] and ($n \geq 70$).[7,15]

Most experimentally known molecular MCAs may however be described to first order by *localized* charges, typically at the periphery of the molecule. Examples include three-dimensional alkali halide cluster multianions[16] or (quasi) one-dimensional aliphatic dicarboxylates $^-OOC-(CH_2)_n-COO^-$ ($n = 3-10$).[17]

* To whom correspondence should be addressed. E-mail: manfred.kappes@chemie.uni-karlsruhe.de.
[†] Forschungszentrum Karlsruhe.
[‡] Universität Karlsruhe.
[§] University of Sherbrooke.

10.1021/jp022141o CCC: $25.00
Published on Web 01/18/2003

Correspondingly, first-order properties, like vertical detachment energies, are in accordance with simple electrostatic calculations employing the appropriate localized charge distributions.

Excepting barrier heights, which have been roughly bracketed by comparing photoelectron spectra for different detachment energies, little is known experimentally about the Coulomb barriers themselves. On a theoretical basis, they are expected to be spatially anisotropic, nonlocal, as well as dependent on both the initial and final states. A first attempt toward a more detailed characterization of barrier "surfaces" was described in a recent PES study of the three possible isomers (*ortho-*, *meta-*, and *para-*) of benzene dicarboxylate $C_6H_4(COO^-)_2$, which are electronically stable dianions having the charges localized on the carboxylate group.[18] In this case, the measurements revealed a shift both in detachment energies and barrier heights due to the different intramolecular Coulomb repulsions depending on the relative position of the extra charges within the molecule.[18]

One may thus infer that analogous electronically metastable isomers might have measurably different electron autodetachment rates. In this study, we show, by using a set of electronically metastable tetraanions as model systems that such variations indeed occur and that they can in fact be quite large.

Wang et al. have recently reported the highest known negative electron detachment energy of −0.9 eV in measurements of isolated copper phthalocyanine−tetrasulfonate tetraanion.[19,20] On the basis of our previous studies, such systems might then be expected to undergo measurable tunneling autodetachment at room temperature. Furthermore, it is known that these and related transition metal phthalocyanine−tetrasulfonates (MPc) are synthesized by a procedure which generates a mixture of several constitutional isomeric forms which differ only in the relative positions of their sulfonic groups. These groups account for the excess charges and are mounted on the molecular perimeters. No previous separations of these constitutional isomers have so far been reported. Consequently, we set out to study the electron autodetachment dynamics of two readily available $MPc(SO_3)_4^{4-}$ systems: copper- and nickel-phthalocyanine−tetrasulfonate tetraanions. Both were obtained as the sodium salts and were studied in gas phase via electrospray volatilization from the appropriate polar solutions. In the case of $CuPc(SO_3)_4^{4-}$, we probed only the isomer mixture. In the case of $NiPc(SO_3)_4^{4-}$, which is accessible to proton-NMR characterization, we succeeded in partial isomer separation and were then able to determine autodetachment rates of selected constitutional isomer fractions.

Specifically, this contribution comprises (i) preparation and partial separation using high-pressure liquid chromatography (HPLC) of constitutional isomers of nickel and copper phthalocyanine−tetrasulfonate $NiPc(SO_3)_4^{4-}$ and $CuPc(SO_3)_4^{4-}$ and in the case of NiPc their characterization and assignment using NMR spectroscopy in solution; (ii) electrospray ionization/volatilization of the corresponding tetraanions as well as their high-resolution mass spectroscopic analysis; (iii) determination of photodetachment energies and photoelectron spectra for isomer mixtures of both M = Ni and Cu; (iv) measurements of the room temperature autodetachment rates for the nickel pthalocyanine tetraanion fractions obtained; and last (v) a semiempirical quantum chemical as well as classical electrostatic modeling study of the electron loss kinetics.

2. Methods

2.1. Sample Preparation and Characterization. Copper and nickel phthalocyanine−tetrasulfonate were prepared via the condensation method adapted from Weber and Bush.[21] Briefly this involved the following.

Nickel-Phthalocyanine−Tetrasulfonate Sodium Salt (MW 978). A mixture of nickelous chloride hexahydrate (MW 237.7, 4.4 g, 18.4 mmol), triammonium sulfophthalic acid (MW 297, 10.87 g, 36.6 mmol), ammonium chloride (MW 53, 0.35 g, 6.5 mmol), ammonium molybdate (0.1 g), and urea (MW 60, 10 g, 0.16 mmol) was heated 3 h at 200 °C, triturated with 1N HCl in brine, filtered and washed with water, dialyzed, evaporated to dryness, and oven-dried to give 7.16 g (80% yield) of the nickel phthalocyanine tetrasulfonate. λ_{max} in DMF: 669 nm (ϵ_{max} = 155 000 L mol^{-1} cm^{-1}).

Copper-Phthalocyanine−Tetrasulfonate Sodium Salt (MW 983.5). A mixture of copper diacetate monohydrate (MW 200, 8 g, 40 mmol), triammonium sulfophthalic acid (MW 297, 39.92 g, 134 mmol), ammonium chloride (MW 53, 8 g), ammonium molybdate (40 mg), urea (MW 60, 40 g, 0.64 mmol), and water (10 mL) was heated 4 h at 190−200 °C, triturated with 1N HCl in brine, filtered and washed with water, dialyzed, evaporated to dryness, and oven-dried to give 18.32 g (55% yield) of the copper phthalocyanine tetrasulfonate. λ_{max} in MeOH: 666 nm.

Preparative HPLC separations were performed by means of a Varian ProStar setup equipped with a UV−vis detector and two Rainin pumps on a reverse phase Dynamax Microsorb C18 column of 250 mm length and 4.6 mm internal diameter which was at room temperature. Solvents (water and methanol) were HPLC grade, and the buffer was freshly prepared and the pH adjusted with sodium dihydrogen phosphate (Merck) to be between 5.1 and 5.30 as measured by a Mettler-Toledo MP 225 pH meter. Mixing and degassing of the eluent (25% methanol in aqueous buffer or in pure water) was effected before it was passed through the column which was protected by a Microsorb C18 guard module. The flow rate was usually 20 mL/min. NMR spectra were recorded overnight on an Bruker Avance 300 spectrometer (300 MHz for protons) in DMSO−D_2O solutions (2:1 to 3:1 vol/vol) where the aggregation was inhibited as observed from absorption spectra measured on Varian Cary 500 instrument. The temperature was set at 75 °C and controlled by the variable temperature unit. The HOD peak was irradiated (PRESAT pulse sequence) in the undecoupled spectra.

2.2. Mass Spectrometry and Ion Trapping. All measurements of autodetachment kinetics were performed with a 7 T Fourier transform ion cyclotron resonance mass spectrometer FT-ICR-MS (APEX-II, Bruker Daltonics) equipped with an electrospray ion source (Analytica of Branford). The ions were obtained upon spraying a 0.1 mmol aqueous solution of the tetrasodium salt of $NiPc(SO_3)_4^{4-}$ and $CuPc(SO_3)_4^{4-}$, respectively, at a typical spraying rate of 100 μL/h. The source contains a hexapole (pre)trap storing the ions for 1 s at 10^{-4} mbar. For that reason, the ions are estimated to be thermalized to room temperature. Experimental details have been described recentl.[5] The Penning trap was held at room temperature and at a pressure of 2×10^{-10} mbar. To acquire unimolecular rates, we chose the following experimental sequence:

1. Trapping: ions were trapped "on the fly" and stored in a electrostatic potential well of typically 1.0−1.5 V depth.

2. Isolation: besides the 4-fold charged species of interest, all other ions were removed from the trap by means of resonant rf excitation.

3. Reaction delay: during a period of up to 1000 s, the ions were allowed to undergo unimolecular decay reactions, in this case electron loss. By varying the length of this delay the kinetics of the reaction can be studied.

4. Detection and quench: all ions, precursor and products, were detected after broadband rf excitation and then removed

SCHEME 1

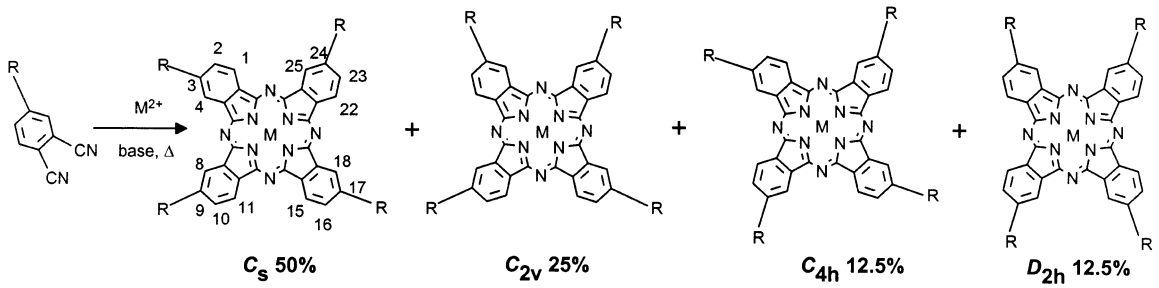

from the trap by pulsing the potential applied to the trapping electrodes of the ICR cell.

This sequence was typically repeated 32 or 64 times, and the data were accumulated in order to achieve a good signal-to-noise ratio. Kinetic data were taken and processed as recently described.[22] Briefly, detected ICR signals from product and educt ions were corrected for their charge state to give relative ion intensities.[23] For single exponential behavior, a unimolecular rate constant k can be determined by fitting a straight line to the logarithmically plotted data, corresponding to the equation

$$\ln(I_t/I_{t=0}) = -kt \qquad (1)$$

where I_t and $I_{t=0}$ denote the intensities of the tetraanion at time t and time 0, respectively.

2.3. Photoelectron Spectroscopy. As-prepared isomer mixtures of $CuPc(SO_3)_4^{4-}$ and $NiPc(SO_3)_4^{4-}$ were probed using a newly constructed magnetic bottle photoelectron spectrometer after Kruit and Read[24] coupled to a reflectron time-of-flight mass spectrometer (RETOF-MS) equipped with an electrospray source and a hexapole trap (Analytica of Branford) as described above. Details of the machine, which is based on a design by Cheshnovsky et al.[25] will be reported elsewhere. Briefly, 0.1 mmol solutions of the respective tetrasodium salts in a mixture of methanol and water (98:2 vol %) were electrosprayed from an off-axis microspray needle using a solution flow rate of 10 μL/min and a drying gas (N_2) temperature of 200 °C. The resulting ions were accumulated for 1/30 s in a hexapole trap at 10^{-4} mbar. As the main gas load in this region stems from the drying gas, we expect the ions to be above room temperature. At the end of each trap period, the ion bunch was extracted and focused into the injection region of the RETOF-MS by an electrostatic lens system. At an appropriate time delay after the trap extraction pulse, ions were accelerated at a starting potential of 485 V in a RETOF-MS perpendicular to the primary ion beam, decelerated to ~30 eV, and irradiated using the third and fourth harmonic of a Nd:YAG laser (Spectra Physics, Quanta RAY series, LAB 150-30). Photoelectrons were collected at nearly 100% efficiency using the magnetic mirror effect in an inhomogeneous magnetic field and allowed to disperse according to their kinetic energy in a 1.68 m drift tube with a weak guiding magnetic field. Electron time-of-flight spectra were acquired by amplifying the electron signal from a double micro channel plate detector in a fast preamplifier and sampling events with a multichannel scaler. The energy axis was calibrated against the well-known photoelectron spectra of I^- at 355 and 266 nm (corresponding to photon energies of 3.49 and 4.66 eV, respectively). The spectra were accumulated over 3×10^5 pulses and corrected for background events due to multiphoton ionization of background gas, electronic noise, etc.

2.4. Computation. Quantum mechanical computations were performed using HyperChem (Release 6.0).[26] First, we optimized the ground-state geometric structure of the $NiPc(SO_3)_4^{4-}$ tetraanions for all four isomers at a semiempirical level (PM3). PM3-Hamiltonians have been shown to give good descriptions of structural properties of analogous organic as well as organometallic systems.[27]

To obtain a better description of the electronic structure, these PM3 geometry optimizations were followed by a single-point calculation at the ZINDO/S, restricted Hartree−Fock level. This INDO (intermediate neglect of differential overlap) method has been parametrized[28] to reproduce electronic properties (like orbital energies and UV−vis spectra) in comparable systems. The tetraanions were calculated as closed shell spin singlets, whereas trianions are expected to have one unpaired electron (spin doublet). The vertical electron detachment energies were taken as the differences between the restricted HF total energy of the quadruply and triply charged ion (at ZINDO/S level), both taken at the optimized geometric structure of the 4-fold charged species. Further classical electrostatic modeling was performed using the software package Mathematica (version 4.0).

3. Results and Discussion

3.1. Sample Preparation and Isomer Separation. Two methods exist for preparing polysulfonated phthalocyanines ($MPc(SO_3)_n^{n-}$): (i) direct sulfonation of a Pc metal complex and (ii) condensation of adequately functionalized derivative of phthalic acid, such as the dinitrile, diamide, anhydride, or diiminoisoindoline also bearing a sulfonated group (usually as the sodium salt) in the presence of a metal salt and base. The latter reaction is depicted in Scheme 1 for the case of the dinitrile bearing a 4-substituent ($R = SO_3^-Na^+$). The percentages listed beside the symmetry point group, to which each isomer belongs, indicate the expectation for the statistical formation of the four possible isomers. It is generally thought that the templating metal ion has a strong influence upon the isomeric distribution which may deviate significantly from the statistical outcome. Also noteworthy is that the condensation method using only one dinitrile precursor yields fewer isomers than are obtained by the direct sulfonation of MPc in which case both the 3- and 4-positions of each *c*-benzo-annulated pyrrole ring become monosubstituted. This was proven by a careful inspection of the rather complex HPLC traces of reaction mixtures obtained by both methods.[29,30] In all previous HPLC studies known to us, the $MPc(SO_3)_4^{4-}$ isomers were always eluted as essentially one peak with a very low retention time, before the corresponding $MPc(SO_3)_3^{3-}$ or $MPc(SO_3)_2^{2-}$ for which an adequate separation of isomers could be achieved.[29]

In this study, we were able to devise a protocol to improve the chromatographic separation of both $CuPc(SO_3)_4^{4-}$ and $NiPc(SO_3)_4^{4-}$ isomeric mixtures obtained by the condensation method. By carefully adjusting the pH (between 5.1 and 5.3) of the phosphate buffer (Na_2HPO_4/NaH_2PO_4) used in conjunction with methanol to elute the isomeric $MPc(SO_3)_4^{4-}$ mixture

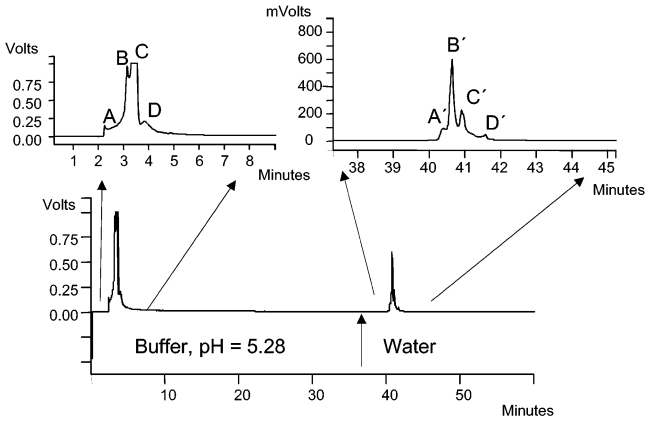

Figure 1. HPLC traces obtained upon applying the protocol (as described in the text) to an isomeric mixture of $NiPc(SO_3)_4Na_4$.

from a reverse phase C18 preparative column, partial separation could be achieved into a rapidly (i.e., with a retention time under seven minutes) eluting cluster of four peaks. In addition to this initial elution, we observed that more $MPc(SO_3)_4^{4-}$ material may be eluted isomer specifically by passing buffer through the column for an extensive time period (up to 120 min) and then rapidly switching the eluent from buffer/methanol to water/methanol (i.e. from pH 5.5 to pH 7.0). Subsequently, a second cluster of peaks (labeled A′, B′, C′, and D′ in Figure 1) is detected and various phthalocyaninic fractions can be collected. The separation of these later eluted peaks is dependent on the pH of the buffer, on the buffer washing time, and on the methanol:buffer, or methanol:water ratio of the eluent. This makes an optimization of such a multiparametric separation tedious. We could not achieve baseline separation for all four isomers in the final cluster of four peaks. However, one component (fraction A′), which according to the ^{1}H NMR for the $NiPc(SO_3)_4^{4-}$ isomeric mixture is the main component (about 50%), could be obtained in a purity over 95%. Similarly, from the cluster of early buffer-eluted peaks, one component was obtained in almost pure form again according to ^{1}H NMR. We cannot exclude that, beside the usual adsorption/desorption equilibria on the nonpolar stationary phase, two other equilibria, namely, aggregation/deaggregation and counterion pairing or protonation (i.e., $SO_3^-Na^+/SO_3H$), occur concomitantly, during the pH ramping phase from the buffer to water eluents.

Evidence for strong aggregation in such solutions comes both from UV−vis[31] and ^{1}H NMR spectroscopic studies. Conditions where the formation of dimers and higher aggregates is largely inhibited, thus allowing finely resolved ^{1}H NMR spectra to be recorded, are the following: dilute (i.e., 10−100 μmolar concentrations) in a D_2O/DMSO-d_6 solution (1:2 to 1:3, vol:vol) and at 75 °C. Because of the low concentrations, usually overnight accumulation of the proton spectra, using a solvent suppression pulse sequence (PRESAT, with irradiation of the residual HOD signal) had to be employed, to achieve a satisfactory signal-to-noise ratio which allowed the assignment of signals, as indicated in Figure 2a. Although in water the H aggregate is predominant, addition of DMSO and increased temperature clearly lead to monomerization.

A detailed ^{1}H NMR study including 2D-COSY and homodecoupling experiments was undertaken with the first eluted fraction after changing the eluent (A′ in Figure 1). The latter spectra are shown in Figure 2b and allow an unambiguous assignment of this component, isolated in about 95% purity, to the C_{2v} isomer. Thus, the high field doublet at 8.55 ppm, with a 6.6 Hz splitting, is assigned to protons situated in β position to the sulfonic group, whereas the two low field signals must

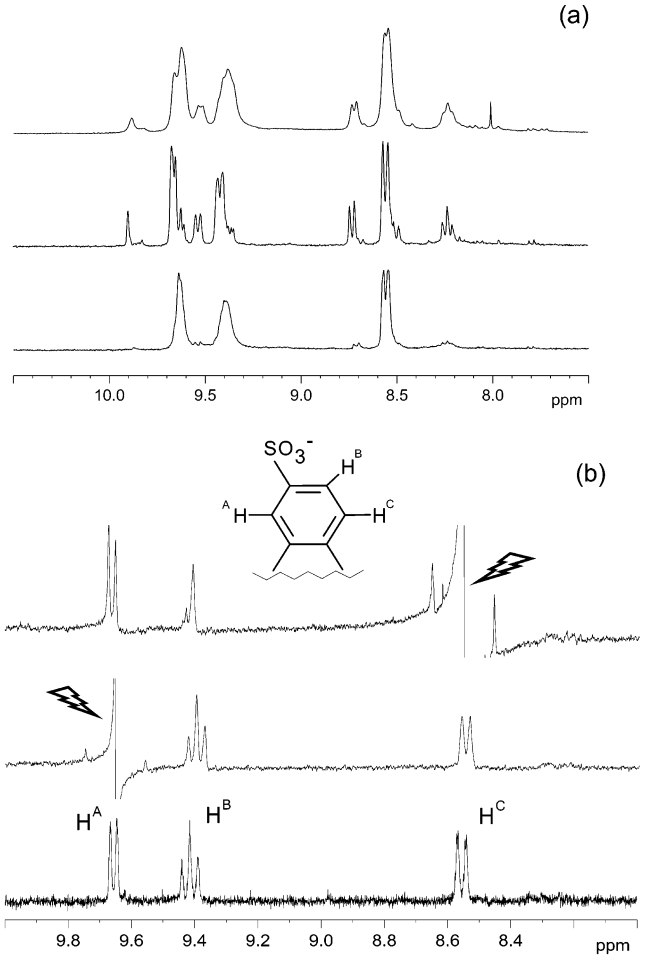

Figure 2. ^{1}H NMR spectra of $NiPc(SO_3)_4Na_4$ solutions: (a) Isomer mixture (upper trace), HPLC-separated fractions B + C (middle trace) and A′ + B′ (lower trace). Note that fine splittings are not observed due to Presat pulse sequence; (b) Decoupling ^{1}H NMR spectra of fraction A′ + B′ without irradiation (lower trace) and irradiating proton H^A (middle trace) and H^B (upper trace).

be in adjacent α positions. As the 9.40 ppm signal is much broader, here the 6.6 Hz coupling must be operative so this signal can be assigned to the proton adjacent both to the sulfonic group and the other 8.55 ppm resonating proton. The sharper, lowest field proton (at 9.64 ppm) is thus the proton between the sulfonic and quaternary phthalocyaninic carbon, in accord with simple estimations of chemical shifts of a trisubstituted benzo-annulated ring-current bearing aromatic moiety. The large 6.6 Hz vicinal coupling is clearly seen in the H−H COSY spectrum from the cross-peak which correlates the 8.55 ppm signal to the 9.40 ppm signal. Revealingly, upon irradiation of the high field doublet, while the 9.4 signal sharpens, two distinct singlets, of equal intensity, are obtained for the low field signal. On the other hand, upon irradiation of the latter signal which leads to cancellation of the small J^4 and J^5 couplings, the broad 9.4 Hz signal becomes a triplet (i.e., two doublets with 7.8 and 8.1 Hz splitting having the middle line superimposing), whereas the high field doublet becomes sharp, showing a 7.8 Hz splitting. This proves that, although the high field protons are in the (almost) same magnetic environment at 300 MHz, two equal populations exist for the other two protons which are adjacent to the sulfonic group. Only the C_{2v} isomer fulfills this requirement. An alternative interpretation could be that this fraction consists of a 1:1 mixture of the D_{2h} and C_{4h} isomers. However, this is a much less probable case.

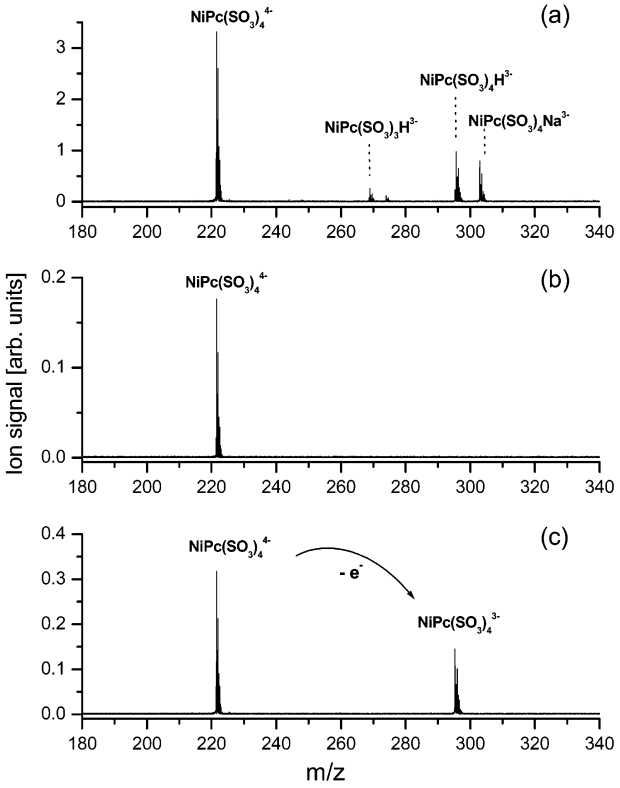

Figure 3. Experimental sequence used to take kinetic data for electron auto-detachment from isolated $NiPc(SO_3)_4^{4-}$: (a) Negative ion ESI−FT−ICR mass spectrum of Ni-phthalocyanine−tetrasulfonate solution. (b) Same as in part a after ejection of all unwanted ions from the trap by means of resonant RF excitation. (c) Mass spectrum taken after a set delay time under UHV.

3.2. Gas-Phase Studies: Mass Spectrometric Analysis and Metastable Decay of $MPc(SO_3)_4^{4-}$. Figure 3a displays a typical negative ion FT-ICR mass spectrum upon spraying an aqueous solution of the isomer mixture of $Na_4[NiPc(SO_3)_4]$. The strongest ICR signal stems from the 4-fold negatively charged $NiPc(SO_3)_4^{4-}$ around *m*/*z* 223. Isotopically resolved mass peaks (not shown here) prove the charge state of all ions described. We also detect $NiPc(SO_3)_4H^{3-}$ and $NiPc(SO_3)_4Na^{3-}$, as well as small amounts of fragments, e.g., $NiPc(SO_3)_3^{3-}$.

Solutions of various isomer fractions (separated by HPLC, see above) were sprayed as obtained from the column and show virtually the same negative ion distributions over the pH range (5.5−7) covered in this study. For fractions C′ and D′, we observe a slightly increased relative intensity of the $NiPc(SO_3)_3^{3-}$peak. Mass analysis of the CuPc−tetrasulfonate solutions revealed the same relative ion intensities, the $CuPc(SO_3)_4^{4-}$ ($m/z = 224$) signal being the most abundant.

To study the stability of the observed multiply charged anions, the ion of interest is unambiguously isolated in the ICR cell as described in section 2.2. Although the triply charged species are stable under UHV conditions (10^{-10} mbar), the 4-fold charged anion undergoes metastable decay. For $NiPc(SO_3)_4^{4-}$, the only decay channel observed at room temperature is electron autodetachment

$$NiPc(SO_3)_4^{4-} \rightarrow NiPc(SO_3)_4^{3-} + e^- \qquad (2)$$

This is evidenced in Figure 3c showing the mass spectrum after isolating the tetraanion in the trap and a reaction delay of 150 s. Note that we can rule out a significant contribution of collision-induced electron loss for two reasons: (i) autodetachment studies were always performed at nominal pressures of less than or equal to 10^{-10} mbar and (ii) intentional addition of argon collision gas to the trap at pressures of ca. 10^{-9} mbar gives rise to primarily fragment ion formation under otherwise identical conditions. No such fragmentation was observed under UHV.

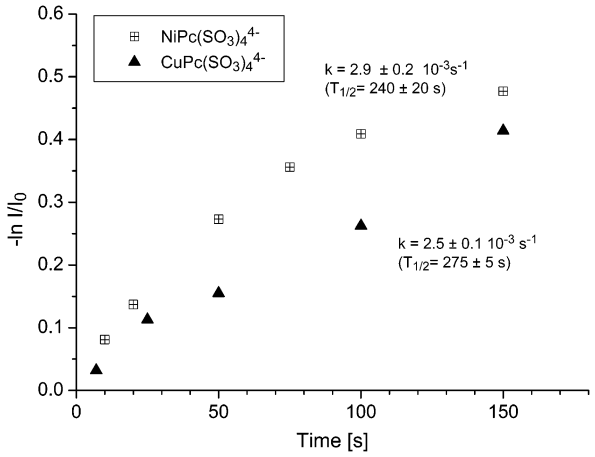

Figure 4. Comparison of experimentally observed electron autodetachment rates for copper and nickel phthalocyanine-tetrasulfonate-tetraanions (isomer ensembles). Rate constants and half-lives are from a linear fit (assuming a unimolecular kinetics) to the data points on the semilogarithmic plot.

Interestingly, electron autodetachment is also observed for $CuPc(SO_3)_4^{4-}$. Figure 4 contrasts the electron autodetachment kinetics of both metallophthalo−cyanine tetraanions in a semilogarithmic plot. Although the data do not exhibit a single exponential behavior, a fact which we interpret is due to the mixture of isomers which are present in the samples in both cases, we formally assign an average half-life to both data sets by a linear fitting procedure. Interestingly, the half-lives differ only slightly as a function of the central metal atom (240s vs 275s for Ni and Cu, respectively). This is consistent with our computational finding (see also next section) that the highest occupied molecular orbital (HOMO) of the NiPc tetraanion essentially resides on the organic moiety with very little contribution from the chelated metal atom. In this context, it is interesting to invoke photoelectron spectra of neutral NiPc and CuPc,[32] where it was shown that lowest energy ionization occurs from the a_{1u} orbital of the Pc ring again with only small variation (<0.1 eV) for different metal atoms. Note also that the photoelectron spectra of the two tetraanions are almost identical as we will show in the next section. Recent DFT calculations support the interpretation that the identity of the central metal atom only plays a minor role in determining the ground-state electronic structure.[33]

To study isomeric effects, various HPLC fractions were subjected to the metastable decay investigations as described in the previous section for the mixture under virtually identical conditions. Figure 5 displays the experimental results for fractions B + C and A′ + B′, for which we identify half-lives of 63 ± 5 s and 2300 ± 100 s, respectively, corresponding to a ratio of 37 ± 5. Kinetic data taken for fractions C′ and D′ indicate the same half-life as A′ + B′. Likewise, fraction C + D shows an electron autodetachment rate comparable to B + C.

According to the NMR assignment fraction A′ + B′ is 95% pure and contains one isomer (C_{2v}). This appears to be considerably more stable with respect to electron autodetachment than the other isomers.

3.3. Gas-Phase Studies: Photoelectron Spectra. Figure 6 contains photoelectron spectra obtained at a detachment wave-

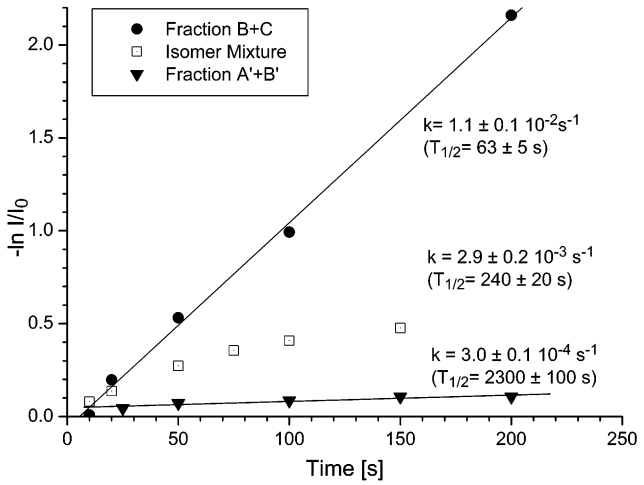

Figure 5. Electron auto-detachment rates for HPLC fractions B and C and A′ and B′ as well as the isomer mixture of $NiPc(SO_3)_4^{4-}$. Note the dramatic difference in rates between the two fractions.

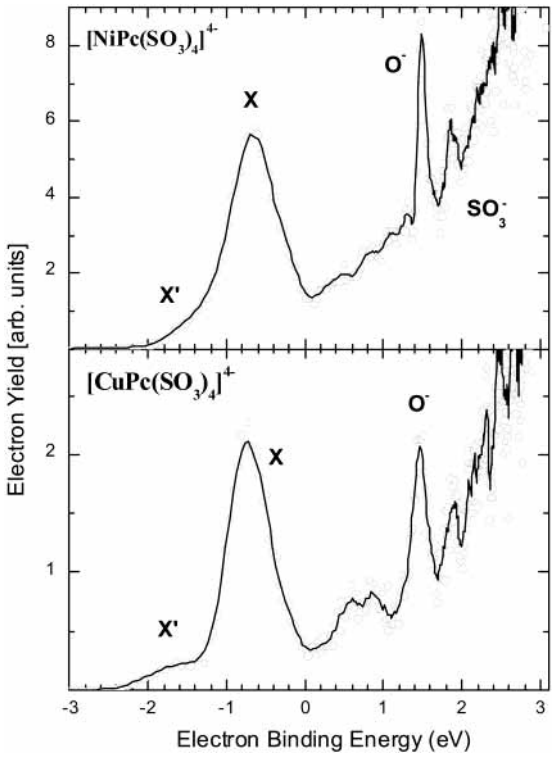

Figure 6. Photoelectron spectra of $NiPc(SO_3)_4^{4-}$ (upper trace) and $CuPc(SO_3)_4^{4-}$ (lower trace) at 355 nm detachment laser wavelength. Each spectrum was obtained by accumulating 3×10^5 shots at a laser fluence of 15 mJ/cm^2. Open circles are measured data points, solid lines are 5 point averaged curves to guide the eye.

length of 355 nm (photon energy 3.49 eV) for both $CuPc(SO_3)_4^{4-}$ and $NiPc(SO_3)_4^{4-}$ isomer mixtures. The spectra look very similar, and we will discuss them using the same labels as in.[20] They both exhibit a pronounced feature at vertical detachment energies (VDE's) around −0.7 eV (labeled X) with a small shoulder at even lower binding energies (X′).

Toward higher binding energies, the spectra exhibit sharp features whose fluence dependence shows that they are clearly related to multiphoton processes, as well as a general increase of the photoelectron yield with increasing binding energy. This is consistent with the observations of Wang et al.[20] that the small signals reported in their spectra could be enhanced by using higher fluences. We tentatively assign the sharp peaks labeled

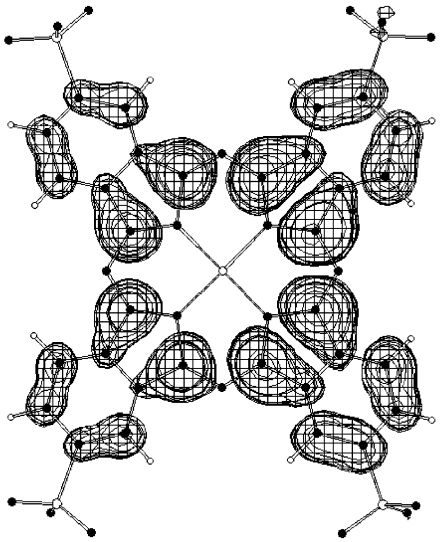

Figure 7. Contour plot of the highest occupied molecular orbital (HOMO) of the D_{2h} isomer of $NiPc(SO_3)_4^{4-}$ from a semiempirical calculation suggesting that the electron most likely to autodetach stems from the delocalized π-electron system of the phthalocyanine molecule.

O^- at 1.48(2) and 1.46(2) eV for Cu and Ni, respectively, to be signatures for the photodetachment from negatively charged atomic oxygen formed by photodissociation of the $MPc(SO_3)_4^{4-}$ ions (the electron affinity of O is 1.4611220(27) eV[34]). Around binding energies of 1.86(3) eV weak features are present which are probably due to photodetachment from SO_3^- generated by photodissociation of $MPc(SO_3)_4^{4-}$ (electron affinity values for SO_3 around 1.9(1) eV have been reported in[35]). Especially, the formation of SO_3^- has been observed in preliminary photodissociation studies that are under way in our group.[36] The observation of strong multiphoton processes at 355 nm is not surprising, as solutions of the metal phthalocyanine salts show strong absorption in this wavelength region. Interestingly, the X′ shoulders toward lower binding energies of the X feature did not show a photon fluence dependent behavior at 355 nm, whereas Wang et al.[20] interpreted a structure observed at the same binding energy in their spectrum taken at 532 nm as being due to a two photon process.

Both X and X′ features are due to photodetachment from $MPc(SO_3)_4^{4-}$, as the respective high electron kinetic energies indicate that they come from a highly charged species, and it is very unlikely that a highly charged species formed in a photodissociation event would retain its charges. However, as outlined in the discussion above, the origin of the X′ band is not quite clear.

On the basis of the photoelectron spectra, we obtain lowest vertical detachment energies (VDE) of −0.71(5) eV and −0.65(5) eV for the Cu and Ni species, corresponding to the energies of the X-band maxima, respectively. Note that the VDE value for our $CuPc(SO_3)_4^{4-}$ spectrum corresponds exactly to that in the spectra of Wang et al.[20] To first order, VDE corresponds to the energy difference between (electronically metastable) tetraanion and trianion in the 4 equilibrium structure.

3.4. Computational. *3.4.1. Ground-State Structure and Energetics.* Semiempirical calculations were performed in order to determine geometric structures and electron detachment energies for the four possible isomers of NiPc. The relaxed geometry of the D_{2h} isomer of $NiPc(SO_3)_4^{4-}$ shown in Figure 7 is an example of results obtained. Except for the four $-SO_3^-$ groups the molecule is essentially planar. The relevant geometrical parameters, like the sulfur−nickel distances, the angle

TABLE 1: Ground State Energetics and Structural Parameters of the Four Possible Isomers of $NiPc(SO_3)_4^{4-}$ [a]

isomer	E_{HOMO} [eV] [b]	VDE [eV] [c]	R(Ni−S) [pm] [d]	S−Ni−S angle [degrees]			
C_s	0.80	−1.16	836 ± 3	69.2	88.7	90.7	111.5
C_{2v}	0.79	−1.16	836 ± 3	89.2	68.6	89.9	112.3
C_{4h}	0.83	−1.17	836 ± 2	90.3	90.2	89.1	90.4
D_{2h}	0.83	−1.17	838 ± 3	69.9	109.2	69.8	111.1

[a] Geometries were optimized using a PM3-Hamiltonian, whereas energies are based on ZINDO/S wavefunctions (see text for details). [b] Energies of the highest occupied molecular orbital (HOMO) as depicted in Figure 5 for the D_{2h} isomer. According to Koopmans' theorem they equal the negatives of the electron binding energy. [c] Vertical electron detachment energy taken as the difference of total electronic energies between the quadruply charged and triply charged anions, both in the frozen equilibrium geometry of the tetraanion. [d] Average of the four nickel−sulfur distances.

between sulfur, nickel, and the adjacent sulfur, are given for all isomers in Table 1.

The PM3-optimized geometries of the four $NiPc(SO_3)_4^{4-}$ isomers were used to calculate electron detachment energies by means of ZINDO/S single-point calculations. Table 1 summarizes the energy eigenvalues of the HOMO (which correspond to the negatives of the electron affinities or electron binding energies according to Koopmans' theorem) as well as vertical detachment energies for all isomers. The negative electron binding energies predict the metastability of the tetraanions with respect to electron loss; differences between the various isomers, however, are not pronounced. On this basis, we would therefore not expect to observe strong isomer dependences in the threshold regions of photoelectron spectra.

Also shown in Figure 7 is a density plot (as given by the square of the HOMO wave function) mapped onto a 3D isosurface. The HOMO is clearly located on the organic ring system with virtually no contribution from the metal atom or the $-SO_3^-$ groups. Rather, the $-SO_3^-$ groups act as localized charge carriers as has been proposed recently for $CuPc(SO_3)_4^{4-}$.[20] This implies that the Coulomb barrier involved in electron autodetachment is determined by these four localized charges, suggesting an electrostatic point charge picture to model the barrier. Figure 8 shows the corresponding electrostatic potential.

3.4.2. Thermal Electron Emission versus Electron Tunneling—A Point Charge Model. As already pointed out in the Introduction, one can think about the electron emission of multiply charged species in terms of two mechanistic limits: thermal electron emission over the Coulomb barrier and tunneling through the Coulomb barrier. In the following, we describe which pathway dominates the room-temperature decay of selected $Ni(Pc(SO_3)_4)^{4-}$ species.

3.4.2.1. Thermal Emission. It is possible to estimate a thermal electron loss rate on the basis of the Klots' theory.[37] This is based on the thermionic emission of solids as given by the Richardson−Dushman equation. The electron emission rate in Klots' theory is given as

$$k(E_0) = 2\frac{k_b T}{h}\frac{Q_{vib}}{Q_{vib}^0}\frac{Q_{el}}{Q_{el}^0}\left(2\frac{b}{a_0} + Q_s + \sqrt{\pi Q_s}\right)e^{-E_0/k_B T} \quad (3)$$

where $Q_s = 2m_e b^2 k_B T/\hbar$ describes the surface of the molecular ion (where m_e denotes the electron mass and b the classical hard sphere collision radius), Q_{vib}, Q_{vib}^0, Q_{el}, and Q_{el}^0 correspond to the vibrational and electronic partition functions after and before the emission, a_0 is the Bohr radius, k_B is the Boltzmann constant, h ($\hbar$) is the (reduced) Planck constant, and

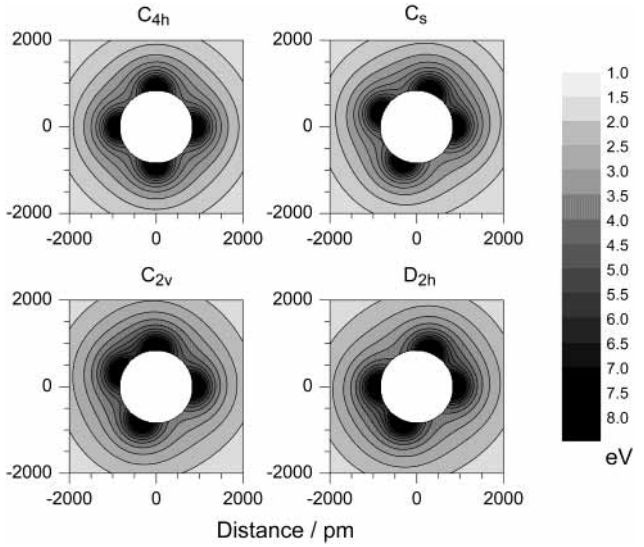

Figure 8. Contour plots of the electrostatic potential in the plane of the molecule for all four $NiPc(SO_3)_4^{4-}$ isomers. One can see the position of the four negative charges at the position of the SO_3^- groups and the preferential tunneling pathways with low barrier heights right between the charges. The potential is cut off at a radius of 837 pm (the mean Ni−S distance).

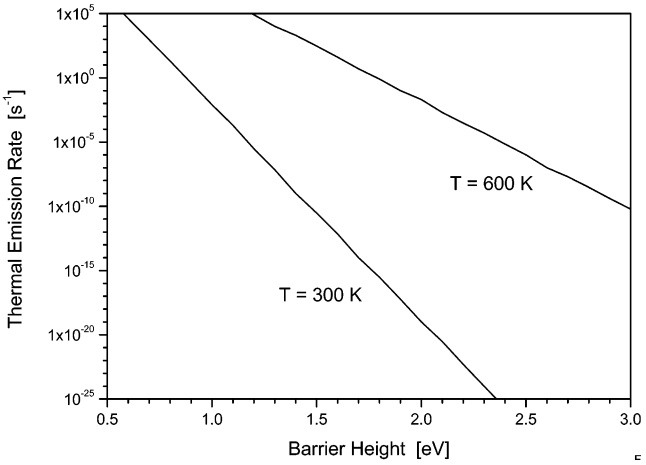

Figure 9. Thermal electron emission rates according to Klots theory (as given in eq 4) for two different temperatures as a function of barrier height. Parameters are conservatively chosen to overestimate the emission rate (see text for details).

T is the temperature of the microscopic system. In the (Coulomb barrier free) case of monoanions, E_0 is the vertical detachment energy, whereas here, we identify E_0 with the height of the Coulomb barrier. The electron loss rates can thus be approximated assuming that Q_{vib} does not change dramatically upon changing the charge state. Because the electronic ground state of the triply charged ion is a doublet, Q_{el} is a factor of 2 bigger than for the spin singlet electronic ground state of the tetraanion.

Figure 9 displays the electron emission rate (according to eq 3) for two different temperatures as a function of barrier height E_0 for a sphere with a radius b of 500 pm. We choose these numbers to ensure that we overestimate the rates for thermal electron emission.

Up to now there are no experimental or theoretical accounts of E_0 for this tetraanion. We note, however, that for the analogous $CuPc(SO_3)_4^{4-}$, Wang et al. estimated a barrier height of about 3.5 eV [20]. As a lower bound for the Coulomb barrier amplitude, one might consider the electrostatic potential that

an outgoing electron (as a point test charge) experiences at a distance of 1.0 nm from the center of the molecule (and thereby well beyond the "geometric" border of the molecule). This yields a value of 2.8 eV (after subtracting the vertical detachment energy of 0.7 eV) as a lower bound for the barrier, which corresponds to an electron emission rate at 600 K of 10^{-8} s^{-1}, about 6 orders of magnitude smaller than the experimentally observed rates.

This estimation indicates that the measured electron loss rates cannot be explained in terms of thermal processes where the electron escapes by means of surmounting the repulsive Coulomb barrier. Apparently, the observed phenomena are primarily due to electron tunneling.

3.4.2.2. Electron Tunneling. To give a semiquantitative account of the different lifetimes in the case of electronic tunneling we developed a simple electrostatic model of the different isomers. It has been shown previously that an electrostatic point charge model is a good approximation to describe the long-range repulsive part of the Coulomb potential in systems characterized by full charge localization[9,22] and gives reasonable results for tunneling rates.[5]

To model $NiPc(SO_3)_4^{4-}$ let us consider a pseudo molecule that is described by an oblate ellipsoid with two equal half-axes R_{mol} (within the plane of the molecule) and one shorter axis Z_{mol} perpendicular to the plane. We now put 4 negative point charges (representing the SO_3^- groups) on the perimeter of a circle with radius R_{mol} and one positive charge in the center (the position of the metal atom). This picture is based on the consideration that the outgoing electron presumably comes from the HOMO which, as already noted above, is mainly located on the frame of the Pc (on the basis of PM3 calculations), resulting in a positive charge at the center of the molecule upon detachment.

Under the further assumption that the bound state of the outgoing electron is set to zero potential, inside the "pseudo" molecule, the resulting potential can thus be written as

$$\phi(\vec{R}) = \begin{cases} 0 & \text{for } \dfrac{R_x^2 + R_y^2}{R_{mol}} + \dfrac{R_z^2}{Z_{mol}} < 1 \\ \dfrac{e^2}{4\pi\epsilon_0}\left(\sum_4^{i=1} \dfrac{1}{|\vec{r}_i - \vec{R}|} - \dfrac{1}{|\vec{R}|}\right) & \text{else} \end{cases} \quad (4)$$

where $e^2/4\pi\epsilon_0 = 1440$ eV pm, the Coulomb potential and r_i are the positions of the negative point charges on the circle with $|r_i| = R_{mol}$ and $R_z = 0$.

Outside, the electron experiences the electrostatic potential of the remaining (overall triply charged) molecular ion. For R_{mol}, we used 837 pm corresponding to a mean Ni−S distance from PM3 calculations (cf. Table 1). The vertical dimension of the molecule (described by Z_{mol}) is set to 150 pm.[38] Both parameters are of course somewhat arbitrary, and the absolute rates are quite sensitive to their variation. However, the *relative* tunneling rates of the different isomers stay nearly the same upon such variation (as long as the bound state energy remains unchanged). The negative charges were positioned on the circumference so as to take into account the angles between the SO_3^- groups in the optimized PM3 structure (cf. Table 1) and are assumed to reside at the position of the sulfur atoms.

Figure 8 shows contour plots (within the molecular plane) of the resulting electrostatic potentials for the four different possible constitutional isomers of $NiPc(SO_3)_4$.[4−] Note that on the basis of these diagrams, besides the pathway perpendicular to the plane of the molecule (which has the same electrostatic potential and thus the same rate for all isomers [38]), the only tunneling pathway which is expected to show significant rate must lie in the plane of the molecule.

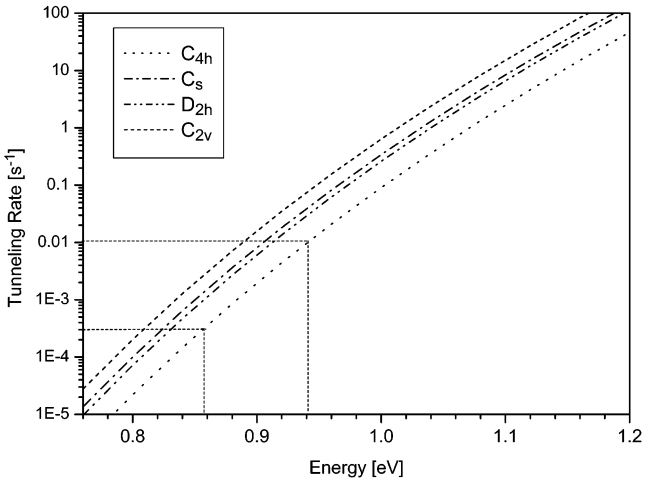

Figure 10. Mean electron tunneling rates for $NiPc(SO_3)_4^{4-}$ isomers (according to eqs 5 and 6) versus energy released in rxn.2 (= −VDE). Isomer specific barrier surfaces are based on the point charge model (eq 4).

According to the WKB approximation[39] one can now calculate a tunneling rate through the barrier by multiplying the tunneling probability with a preexponential attempt frequency. Following the textbook treatment of ref 4, we assume this attempt frequency may be calculated by (i) setting −VDE equal to the kinetic energy of the detaching electron within the model potential and (ii) equating the attempt frequency with $1/t_{coll}(R)$ where $t_{coll}(R)$ corresponds to the time required for an electron with this kinetic energy to travel a distance 2R. This leaves us with eq 5:

$$k(E) = \frac{\sqrt{2E/m}}{2R} \exp\left\{-\frac{2}{\hbar}\int_{R'}^{R} \sqrt{2m(V(x) - E)}\, dx\right\} \quad (5)$$

$V(x)$ is the potential barrier and R and R' are the integration limits, corresponding to the respective "inside" and "outside" separations (as measured from the molecular origin) at which the Coulomb energy becomes equal to the kinetic energy E of the outgoing electron. In this approximation, the latter is also taken as (−VDE) tetraanion.

The WKB theory describes the one-dimensional tunneling problem. Therefore, we calculated one-dimensional cuts going radially outward from the origin of the pseudomolecule. The direction is described by the two angles θ and ϕ in a spherical coordinate system. We end up with an expression for the tunneling rates, $k(\theta,\phi)$. For the following discussion, we use a mean tunneling rate obtained by integrating over the entire solid angle:

$$\bar{k} = \frac{1}{4\pi}\int_0^{2\pi}\int_0^{\pi} k(\theta,\phi)\sin\theta\, d\theta\, d\phi \quad (6)$$

Note that in calculating $\bar{k}$ for our model ellipsoid, R is fully determined by a specific combination of angular coordinates. Figure 10 shows the mean tunneling rate as a function of the energy released in reaction 2 (−VDE) calculated with the parameters described above for all four isomers. We note again that the potential perpendicular to the molecular plane is independent of the position of the negative charges (and

therefore of the various isomers), so we restrict ourselves to discussing differences of the potential within the plane of the molecule.

We see that for the same VDE there is a factor of 4−10 difference (depending on the exact cut off value in *z* direction) in the rate between the fastest decaying isomer (C_{2v}) and the slowest one (C_{4h}). This is in apparent contradiction to the experimental finding (using the NMR assignment) that the C_{2v} isomer exhibits the smallest rate. However, Figure 10 also reveals that the tunneling rate should strongly depend on the VDE, which has previously been seen in the case of $PtCl_xBr_{4-x}^{2-}$.[22] This is a consequence of the $\exp[-\sqrt{[V(x) - E]}]$ dependence. For the same isomer, the experimentally observed range in tunneling rates (marked by the dashed lines in Figure 10) would correspond to a variation in electron detachment energy of only 0.08 eV. These small differences are certainly beyond the accuracy of our semiempirical calculations. Furthermore, vibrational coupling is expected to play an important role in such processes and has not been considered in our simple model.

Consequently, with the computational resources currently available to us (DFT calculations of multianions turn out to be problematic), we can only state that the observed rate variations are plausible and quantitatively consistent with the proposed tunneling mechanism. We cannot yet predict isomer specific tunneling rates computationally. The NMR assignment together with our model argues that in this specific system there are two factors of roughly equal magnitude which contribute to the isomer dependence: slight variations in detachment energies on the order of 0.1 eV as well as changes to the barrier surface because of the relative positions of the excess charges. It is not yet clear how these are correlated. Interestingly though, if we assume that potential surface and attempt frequency are correctly described, the observed absolute electron tunneling rates predict an electron detachment energy that lies between the values obtained by Koopmans' theorem and computed vertical detachment energies (see Table 1).

4. Conclusions

Spontaneous electron loss from $Ni(Pc(SO_3)_4)^{4-}$ and $Cu(Pc(SO_3)_4)^{4-}$ was studied in a UHV Penning trap at ambient temperature. The influence of the metal atom on the (average) rate constants of electron autodetachment was found to be negligible. This is consistent with photoelectron spectroscopic measurements of the respective lowest vertical detachment energies of the corresponding constitutional isomer ensembles which were virtually identical. However, in the case of the nickel system (for which partial isomer separation and proton-NMR characterization was possible), a strong dependence of the unimolecular detachment rate on individual constitutional isomer structure was found. The corresponding rate constants were found to vary by a factor of 37 (3×10^{-4}−10^{-2} s^{-1}) for (partially) separated isomer fractions. Isomers differ essentially only by the position of the sulfonate ($-SO_3^-$) groups, carrying the excess charge, which are mounted on the molecular perimeter. The lowest measured electron loss rate was assigned to the C_{2v} isomer on the basis of ^1H NMR.

Estimates based on Klots theory for thermal electron emission, indicate that in such systems predicted unimolecular rates at room temperature are many orders of magnitude below the experimentally observed ones. As a corollary, electron emission from $Ni(Pc(SO_3)_4)^{4-}$ is attributed to electron tunneling through the Coulomb barrier surface formed by the four excess charges. A simple electrostatic model was used to describe the Coulomb barriers of the four isomers, and electron loss rates were calculated on the basis of the Wentzel−Kramers−Brillouin (WKB) approximation. The differences in the repulsive Coulomb barriers cannot solely account for the different electron loss rates. According to the electrostatic model, the C_{2v} isomer has the smallest barrier height and should therefore be the least kinetically stable isomer, everything else being equal. However, the tunneling rate is also a sensitive function of the electron detachment energy, with differences on the order of 0.1 eV leading to comparable variations in autodetachment rate.

At this point, it is not feasible to compute electron detachment energies with high enough precision using ab initio quantum chemical methods. According to our experiments, the electron detachment energy should be lower for the C_{2v} isomer than for the other isomers. It will be of great interest to verify these isomer specific values by highly resolved photoelectron spectroscopy on pure isomer fractions. This requires an improved HPLC separation procedure in order to prepare the necessary amounts of material, an improvement in photoelectron spectrometer energy resolution and finally, decreased vibrational excitation levels in the tetraanions probed.

We have however demonstrated here that, for electronically metastable multianions with charges localized on their molecular perimeters, isomer differentiation is possible on the basis of their (differing) electron autodetachment rates. This may be of interest for temperature-dependent probes of isolated biomolecules and polymer conformational dynamics in which localized negative charges play a role.

Acknowledgment. This research was partially supported by DFG-CFN and Sonderforschungsbereich 195.

References and Notes

(1) Schauer, S.; Williams, P.; Compton, R. N. *Phys. Rev. Lett.* **1990**, *65*, 625.
(2) Blades, A. T..; Kebarle, P. *J. Am. Chem. Soc.* **1994**, *116*, 10761.
(3) Wang, X.-B.; Nicholas, J. B.; Wang, L.-S. *J. Chem. Phys.* **2000,** *113*, 10837.
(4) Wang, X.-B.; Wang, L.-S. *Phys. Rev. Lett.* **1999**, *83*, 3402.
(5) Weis, P.; Hampe, O.; Gilb, S.; Kappes, M. M. *Chem. Phys. Lett.* **2000**, *321*, 426.
(6) Wang, L.-S.; Wang, X.-B. *J. Phys. Chem. A* **2000**, *104* , 1978.
(7) Compton, R. N.; Tuinman, A. A.; Klots, C. E.; Pederson, M. R.; Patton, D. C. *Phys. Rev. Lett.* **1997**, *78*, 4367.
(8) Yannouleas, C.; Landman, U. *Chem. Phys. Lett.* **1994**, *217*, 113.
(9) For a recent review on gas-phase multianions, see: Dreuw, A.; Cederbaum, L. S. *Chem. Rev.* **2002**, *102*, 181.
(10) Dreuw, A.; Cederbaum, L. S. *Phys Rev. A* **2001**, *63*, 049904(E).
(11) Yannouleas, C.; Landman, U.; Herlert, A.; Schweikhard, L. *Phys. Rev. Lett.* **2001**, *86*, 2996.
(12) Stoermer, C.; Friedrich, J.; Kappes, M. M. *Int. J. Mass Spectrom.* **2001**, *206*, 63.
(13) Hettich, R. L.; Compton, R. N.; Ritchie, R. H. *Phys. Rev. Lett.* **1991**, *67*, 1242.
(14) Limbach, P. A.; Schweikhard, L.; Cowen, K. A.; McDermott, M. T.; Marshall, A. G.; Coe, J. V. *J. Am. Chem. Soc.* **1991**, *113*, 6795.
(15) Hampe, O.; Neumaier, M.; Blom, M. N.; Kappes, M. M. *Chem. Phys. Lett.* **2002,** *354*, 303.
(16) Friedrich, J.; Weis, P.; Kaller, J.; Whetten, R. L.; Kappes, M. M. *Eur. Phys. J. D* **1999**, *9*, 269.
(17) Wang, L.-S.; Ding, C.-F.; Wang, X.-B.; Nicholas, J. B. *Phys. Rev. Lett.* **1998**, *81*, 2667.
(18) Wang, X.-B.; Nicholas, J. B.; Wang, L.-S. *J. Chem. Phys.* **2000**, *113*, 653.
(19) Wang, X.-B.; Wang, L.-S. *Nature* **1999**, *400*, 245.
(20) Wang, X.-B.; Ferris, K.; Wang, L.-S. *J. Phys. Chem. A* **2000**, *104*, 25.
(21) Weber, J. H.; Bush, D. H. *Inorg. Chem.*, **1965**, *4*, 469.
(22) Blom, M. N.; Hampe, O.; Gilb, S.; Weis, P.; Kappes, M. M. *J. Chem. Phys.* **2001**, *115*, 3690.
(23) Marshall, A. G.; Hendrickson, C. L.; Jackson, G. S. *Mass Spec. Rev.* **1998**, *17*, 1.

(24) Kruit, P.; Read, F. H. *J. Phys. E: Sci. Instrum.* **1983**, *16*, 313.
(25) Cheshnovsky, O.; Yang, S. H.; Pettiette, C. L.; Craycraft, M. J.; Smalley, R. E. *Rev. Sci. Instrum.* **1987**, *58*, 2131.
(26) HyperChem Release 6.0, Hypercube Inc. 1999.
(27) Kurtz, H. A.; Stewart, J. J.; Dieter, K. M. *J. Comput. Chem.* **1990**, *11*, 82.
(28) Ridley, J. E.; Zerner, M. C. *Theor. Chim. Acta* **1976**, *42*, 223. Bacon, A. D.; Zerner, M. C. *Theor. Chim. Acta* **1979**, *53*, 21.
(29) Ali, H.; Langlois, R.; Wagner, J. R.; Brasseur, N.; Paquette, B.; van Lier, J. E. *Photochem. Photobiol.* **1988**, *47*, 713.
(30) Ambroz, M.; Beeby, A.; MacRobert, A. J.; Simpson, M. S. C.; Svensen, R. K.; Phillips, D. *J. Photochem. Photobiol. B: Biol.* **1991**, *9*, 87.
(31) Balaban, T. S. To be published.
(32) Berkowitz, J. *J. Chem. Phys.* **1979**, *70*, 2819−2828.
(33) Liao, M.-S.; Scheiner, S. *J. Chem. Phys.* **2001**, *114*, 9780.
(34) Andersen, T.; Haugen, H. K.; Hotop, H. *J. Phys. Chem. Ref. Data* **1999,** *28*, 1511.
(35) Bartmess, J. E. Negative Ion Energetics Data. In *NIST Chemistry WebBook, NIST Standard Reference Database, 69*; Linstrom, P. J., Mallard, W. G., Eds.; National Institute of Standards and Technology: Gaithersburg, MD, 2001; http://webbook.nist.gov.
(36) Ehrler, O. T.; Weber, J. M.; Kordel, M.; Hampe, O.; Kappes, M. M. To be published.
(37) Klots, C. E. *Chem. Phys. Lett.* **1991**, *186*, 73.
(38) Because of the prevailing electrostatics, tunneling barriers are much wider in the vertical direction than in the $x-y$ plane. Consequently even though potential maxima in z-direction may be comparable in magnitude to the height of in-plane "saddles", tunnelling along z does not contribute significantly to the overall rate (eq 6) for any of the isomers studied.
(39) Schwabl, F. *Quantenmechanik, 3*. German Edition, Springer-Verlag: New York, 1992